Available online at www.sciencedirect.com
ScienceDirect
Journal of Solid State Chemistry 180 (2007) 2747–2755
JOURNAL OF SOLID STATE CHEMISTRY
www.elsevier.com/locate/jssc

Characterization and physical properties of Li_2O–CaF_2–P_2O_5 glass ceramics with Cr_2O_3 as a nucleating agent—Physical properties

G. Murali Krishna, B. Anila Kumari, M. Srinivasa Reddy, N. Veeraiah*

Department of Physics, Acharya Nagarjuna University - Nuzvid Campus, Nuzvid 521 201, India

Received 28 May 2007; accepted 9 July 2007
Available online 11 August 2007

Abstract

In this paper, studies on various physical properties, viz., dielectric properties (dielectric constant, loss $\tan\delta$, a.c. conductivity σ) over a wide range of frequency and temperature, optical absorption, ESR at liquid nitrogen temperature and magnetic susceptibility at room temperature of Li_2O–CaF_2–P_2O_5: Cr_2O_3 glass ceramics, have been reported. The optical absorption, ESR and magnetic susceptibility studies indicate that the chromium ions exist in Cr^{5+}, Cr^{4+} and Cr^{6+} states in addition to Cr^{3+} state in these samples. The dielectric constant and loss variation with the concentration of Cr_2O_3 have been explained on the basis of space charge polarization mechanism. The dielectric relaxation effects exhibited by these samples have been analysed by a graphical method and the spreading of dielectric relaxation has been established. The a.c. conductivity in the high-temperature region seems to be connected both with electronic and ionic movements.

Keywords: Dielectric properties; Optical absorption; ESR spectra

1. Introduction

This paper is devoted to report the results of a systematic study on dielectric properties (viz., dielectric constant, loss and a.c. conductivity over a wide range of frequency and temperature), optical and magnetic properties of Li_2O–CaF_2–P_2O_5: Cr_2O_3 glass ceramics. The studies on dielectric properties not only help in estimating the insulating strength but also give some additional information on structural aspects of the glass and glass-ceramic materials. Work along these lines has been carried out in recent years on a variety of inorganic glass systems yielding valuable information [1–5]. The objective of this study is to throw some light on the structural aspects of Li_2O–CaF_2–P_2O_5 glass ceramics with Cr_2O_3 as nucleating agent with the investigations on dielectric properties coupled with the data on ESR, optical absorption and magnetic susceptibilities studies.

2. Experimental

For the present study, a particular composition (30–x) Li_2O–10 CaF_2–60 P_2O_5: x Cr_2O_3 with five values of x ranging from 0 to 1.0 is chosen. The details of the compositions as reported in the Part I are:

C_0 : 30 Li_2O − 10 CaF_2 − 60 P_2O_5

C_2 : 29.8 Li_2O − 10 CaF_2 − 60 P_2O_5 : 0.2 Cr_2O_3

C_4 : 29.6 Li_2O − 10 CaF_2 − 60 P_2O_5 : 0.4 Cr_2O_3

C_6 : 29.4 Li_2O − 10 CaF_2 − 60 P_2O_5 : 0.6 Cr_2O_3

C_8 : 29.2 Li_2O − 10 CaF_2 − 60 P_2O_5 : 0.8 Cr_2O_3

C_{10} : 29.0 Li_2O − 10 CaF_2 − 60 P_2O_5 : 1.0 Cr_2O_3

The techniques of the preparation and the characterization of the samples were reported earlier [5]. The optical absorption spectra of the glasses were recorded at room temperature in the wavelength range 300–800 nm up to a resolution of 0.1 nm using CARY 5E UV–VIS-NIR

*Corresponding author. Fax: +91 8656 235200.
E-mail address: nvr8@rediffmail.com (N. Veeraiah).

0022-4596/$ - see front matter © 2007 Elsevier Inc. All rights reserved.
doi:10.1016/j.jssc.2007.07.025

Spectrophotometer. The ESR spectra of the fine powders of the samples were recorded at liquid nitrogen temperature on JEOL JES-TES100 X-band EPR spectrometer. The samples used for optical and dielectric studies were prepared by suitable grinding and optical polishing to the dimensions of 1 cm × 1 cm × 0.2 cm. A thin layer of silver paint was applied on either side of the large-faces of the samples, in order to serve as electrodes for dielectric measurements. The dielectric measurements were made on LCR Meter (Hewlett-Packard Model-4263 B) in the temperature range 30–250 °C. The accuracy in the measurement of dielectric constant is ~0.001 and that of loss is $\sim 10^{-4}$. The magnetic susceptibility measurements were made by Guoy's method using fine powders of the sample to an accuracy of 10^{-6} emu.

3. Results and discussion

3.1. Optical absorption

Fig. 1 shows the optical absorption spectra of Li_2O–CaF_2–P_2O_5: Cr_2O_3 glass ceramics in the wavelength region 300–1500 nm; the absorption edge observed at 314 nm for the sample C_0 is observed to shift to 320 nm with the introduction of nucleating agent (0.2 mol%). When the content of Cr_2O_3 is raised to 0.4 mol%, the edge is observed to shift towards further higher wavelength. When the concentration of the dopant is raised further (up to 0.8 mol%) the edge is gradually shifted towards lower wavelength. From the observed absorption edges, we have evaluated the optical band gaps (E_o) of these samples by drawing Urbach plots (Fig. 1b) between $(\alpha\hbar\omega)^{1/2}$ and $\hbar\omega$ as per the equation,

$$\alpha(\omega)\hbar\omega = c(\hbar\omega - E_o)^2. \quad (1)$$

From the extrapolation of the linear portion of the curves of Fig. 1(b), the values of optical band gap (E_o) are determined and presented in Table 1 along with the other pertinent data. The value of the optical band gap is observed to be the highest for the sample C_8.

The spectrum of glass-ceramic sample C_2 exhibited absorption bands at 452 and 655 nm identified due to the conventional transitions of Cr^{3+} ions. The intensity of these two bands is observed to increase when the concentration of crystallizing agent Cr_2O_3 is raised to 0.4 mol%; additionally two feeble but clear kinks at about 680 and 717 nm have appeared on 650 nm band in the spectra of the samples C_2 and C_4. For further increase in the content of Cr_2O_3 a new band at about 355 nm, identified due to the excitation of CrO_4^{2-} (Cr (VI)) group is observed; a broad band with a meta-center at about 1020 nm could clearly be detected in the spectrum of the ceramic sample C_8, this band is identified due to $^3A_2 \rightarrow {}^3T_2$ transition of Cr^{4+} ions [6]. It may be worth mentioning here that we have recorded the optical absorption spectra of all the samples before crystallization; the spectra have exhibited only the conventional bands of Cr^{3+} ions.

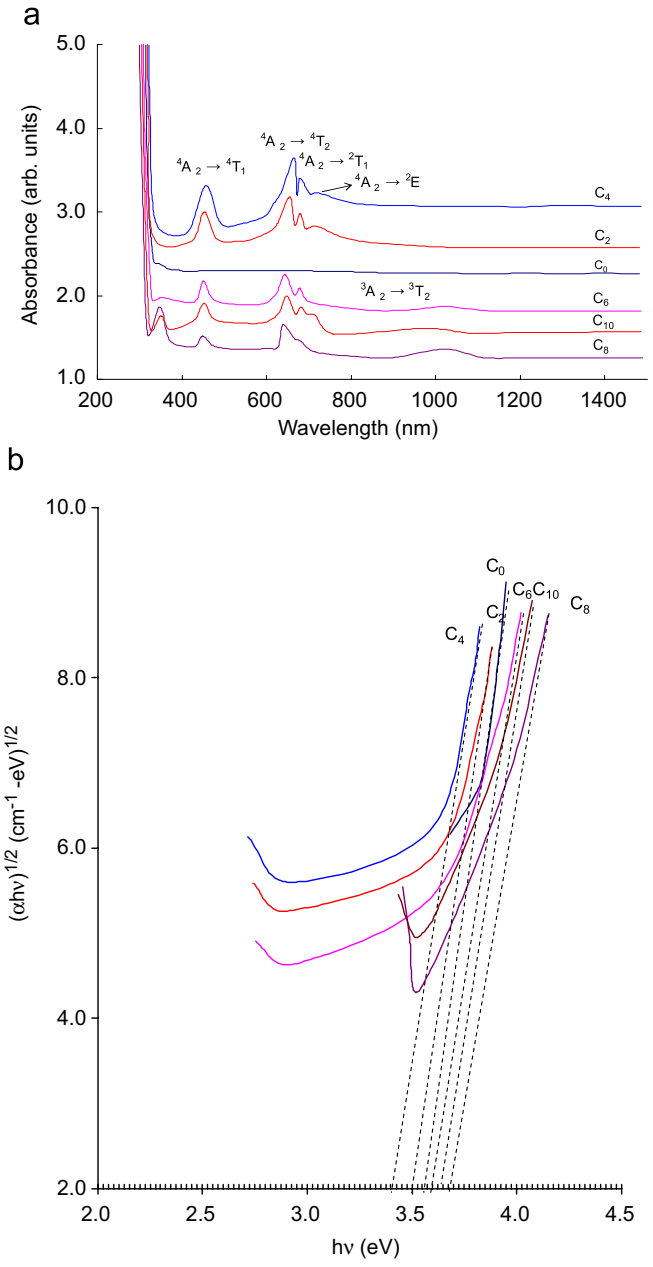

Fig. 1. (a) Optical absorption spectra of Li_2O–CaF_2–P_2O_5: Cr_2O_3 glass ceramics. (b) Urbech plot for evaluating optical band gap of Li_2O–CaF_2–P_2O_5: Cr_2O_3 glass ceramics.

Using Tanabe–Sugano diagrams for d^3 ion, the spectra have been analysed and the bands are assigned to $^4A_2 \rightarrow {}^4T_1$(F), $^4A_2 \rightarrow {}^4T_2$ transitions, respectively. The corresponding LF parameters D_q (crystal field splitting energy) and B (Racah parameter, measure of the Coulomb repulsion among the 3d electrons of Cr^{3+} ion) have been evaluated and presented in Table 1. Using these values, the nephelauxetic ratio, i.e, $\beta = B$ (complex)/B (free ion) is evaluated for all the glasses and also presented in Table 1; the value of β is observed to decrease with gradual increase in the concentration of chromium content in the ceramic sample from 0.4 to 0.8 mol%. These results point out that there is a gradual increase in the covalent environment for

Table 1
Summary of the data on optical absorption spectra of Li_2O–CaF_2–P_2O_5:Cr_2O_3 glass ceramics

Glass	Cut-off wavelength (nm)	Optical band gap E_0 (eV)	Position of $^4A_2 \rightarrow {}^4T_1$(F) band (nm)	Position of $^4A_2 \rightarrow {}^4T_2$ band (nm)	D_q (cm^{-1})	B (cm^{-1})	β
C_0	314	3.55	–	–	–	–	–
C_2	319.4	3.5	452	655	1526	621	0.676
C_4	324.3	3.4	456	664	1504	630	0.686
C_6	308.4	3.575	451	643	1555	610	0.664
C_8	298.7	3.675	449	637	1570	605	0.659
C_{10}	304	3.625	453	648	1543	620	0.675

chromium ions in the glass-ceramic network. Additionally, a pair of weak narrow structures at 687 and 702 nm due to $^4A_2 \rightarrow {}^2T_1$ and $^4A_2 \rightarrow {}^2E$ (spin and parity forbidden) transitions, respectively, have also been located with a clear resolution on $^4T_2$ band in the spectra of samples C_2 and C_4. These bands appear due to the mixing of free ion wave functions with those of neighbour ions or the lattice vibrations. The essential condition for the mixing of free ion wave functions with those of neighbour ions or the lattice vibrations is that the symmetry associated with the centre of inversion is to be destroyed by the neighbours. Further, an increase in the widths of ^2E and $^2T_1$ bands could clearly be seen with a considerable shift towards higher wavelength with increase in the concentration of chromium ions from 0.2 to 0.4 mol%. Such an increase indicates an increase of disorder in the glass network, may be due to the increasing concentration of induced heterogeneous nucleation centres in the glass network that separate and reduce the long-range order of chromium and phosphate groups [7,8]. The optical absorption spectra of the ceramic samples exhibited an additional band at about 350 nm predicted due to the transition of Cr^{6+} ions at the expense of the bands due to Cr^{3+} ions when the concentration of the nucleating agent is increased beyond 0.4 mol%. These Cr (VI) ions exist in the form of $Cr^{6+}O^{2-}$ centres in the frame of CrO_4^{2-} groups [9]. Cr^{6+} ion belongs to d^0 closed shell and does not have electrons in the d shell. Hence, this transition is due to charge transfer or the transformation of chromium ions from Cr^{6+} ($3d^0 2p^6$) state into Cr^{5+} ($3d^1 2p^5$) state. In other words, the observed band is due to the excitation of p electron (involved in the ligand bonds of the $t_1\pi$ symmetry) into the d shell. The energy level of Cr^{5+} ion with $3d^1 2p^5$ electronic configuration splits into two states of symmetry, viz., $2e$ and $4t_2$. In view of this, we may expect two charge transfer bands corresponding to the following transitions from Cr^{6+} ions [10]:

$$CrO_4^{2-}(3d^0 2p^6) \rightarrow CrO_4^{3-}(3d^1 2p^5)(t_1^5, 2e)$$

and

$$CrO_4^{2-}(3d^0 2p^6) \rightarrow CrO_4^{3-}(3d^1 2p^5)(t_1^5, 4t_2).$$

Among these two, the band observed at about 350 nm can be ascribed to the first transition where as the band due to second transition (high-energy transition) band lies well below the cut-off wavelength [10]. Further, the spectrum of the ceramic sample C_8 exhibited a broad absorption hump in the region 900–1100 nm assigned to $^3A_2 \rightarrow {}^3T_2$ transition of tetrahedrally coordinated Cr^{4+} ions [11]. Thus the analysis of the optical absorption spectra together with the XRD and EDS spectra (represented in Part I) point out that there is a possibility for the oxidation of Cr^{3+} ions into Cr^{6+} and Cr^{4+} ions during the crystallization despite the fact the original glass batch contains chromium ions in Cr^{3+} state. As mentioned before, Cr^{3+} ions occupy octahedral positions where as Cr (VI) ion may enter the glass network with CrO_4^{2-} structural units and alternate with PO_4 units. A schematic illustration of phosphate network containing Cr^{3+} (in octahedral and tetrahedral) and Cr^{6+} ions tetrahedral positions is shown in Fig. 2.

The Cr^{3+} ions act as modifier similar to Li^+ and Ca^{2+} ions in the glass-ceramic network. The lower the concentration of these modifier ions, the lower is the concentration of NBOs in the glass matrix. This leads to a decrease in the degree of localization of electrons there by decreasing the donor centres in the glass matrix. The presence of smaller concentration of these donor centres increases the optical band gap and shifts the absorption edge towards low wavelength side as observed (Fig. 1b).

3.2. Fluorescence studies

The fluorescence spectra (Fig. 3) of all the glass-ceramic samples is recorded at room temperature excited at 456 nm; the spectra exhibited a broad emission band in the spectral range of 750–800 nm. This band is identified due to $^4T_1 \rightarrow {}^4A_2$ transition of octahedral Cr^{3+} ions [12]. As the concentration of crystallizing agent is increased from 0.2 to 0.4 mol%, a considerable hike in the intensity of the peak with a shift in the meta-centre towards higher wavelength side could clearly be seen. For further increase in the concentration of Cr_2O_3, the emission band is faded away slowly. Thus the result of luminescence spectra point out that there is a decreasing concentration of Cr^{3+} ions (possibly due to conversion of these ions into Cr^{6+} state) from sample C_4 to C_8.

3.3. ESR spectra

The ESR spectra of Li_2O–CaF_2–P_2O_5: Cr_2O_3 glass-ceramics samples recorded at liquid nitrogen temperature

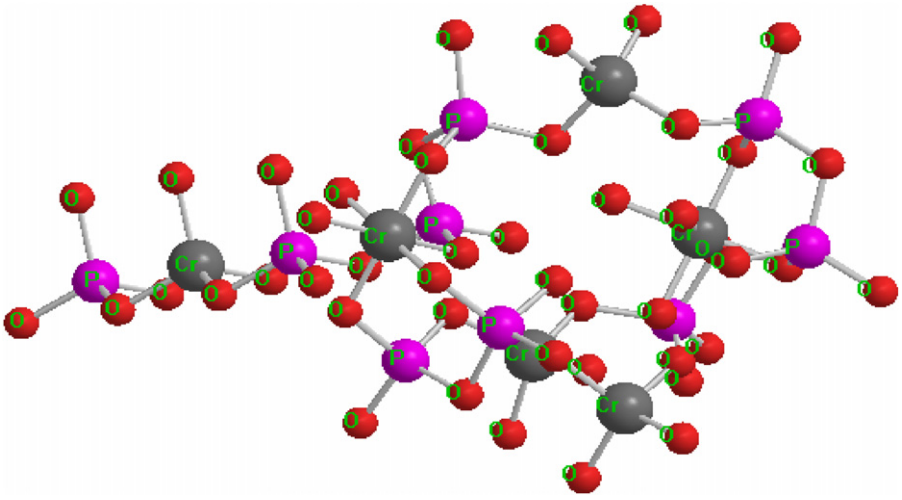

Fig. 2. A schematic illustration of phosphate network containing Cr^{3+} (in octahedral) and Cr^{6+} ions tetrahedral positions in 3D.

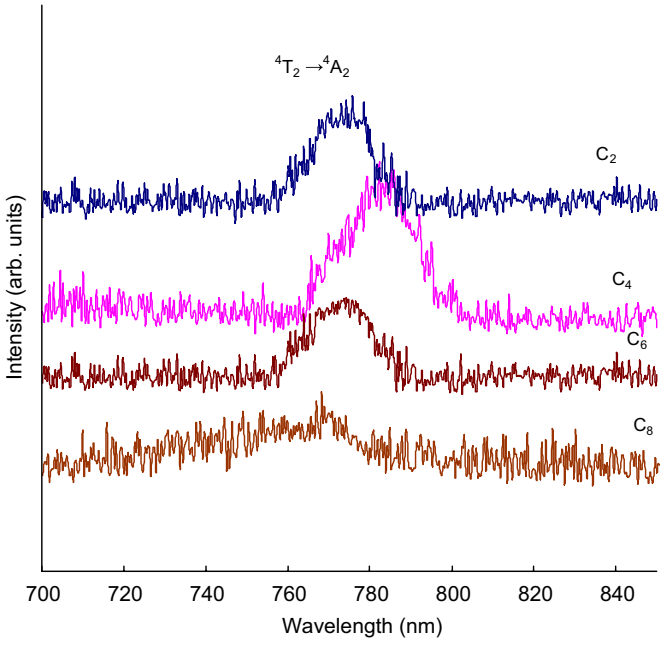

Fig. 3. Luminescence spectra of Li_2O–CaF_2–P_2O_5: Cr_2O_3 glass-ceramics recorded at room temperature with an excitation wavelength of 456 nm.

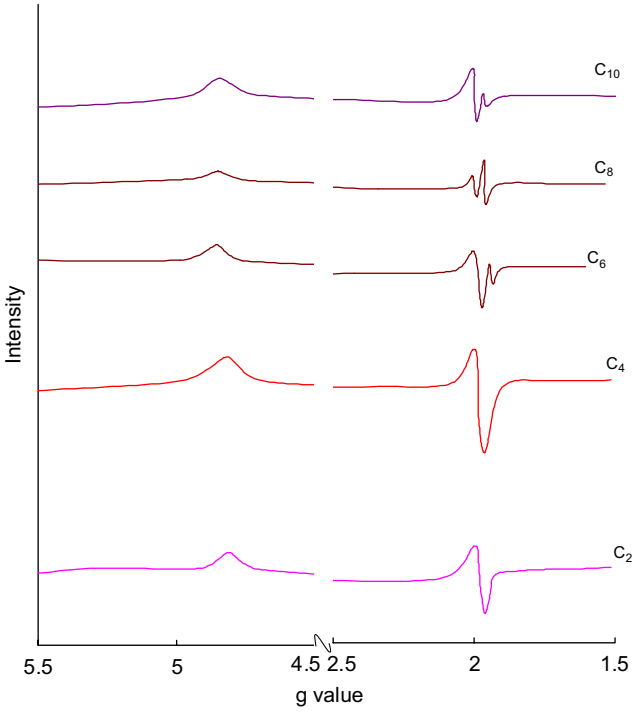

Fig. 4. ESR spectra of Li_2O–CaF_2–P_2O_5: Cr_2O_3 glass-ceramics recorded at liquid nitrogen temperature.

(Fig. 4) exhibit a remarkable dependence on the concentration of chromium ions. The spectra of the C_2 and C_4 ceramic samples showed a strong signal at $g = 1.975$ and a broad signal at about $g = 4.73$ due to Cr^{3+} ions [13,14]. The separation between the two Kramers doublets, viz., $|\pm\frac{3}{2}\rangle$ and $|\pm\frac{5}{2}\rangle$ leads to these two resonances. More precisely, as per the theory of Landry, the low field line at $g \sim 4.7$ is attributed to the isolated Cr^{3+} ions that have local rhombic sites subjected to strong crystal field effects [15,16]. This signal arises mainly due to $-3/2 \leftrightarrow +3/2$, that are allowed due to low symmetry of Cr^{3+} ions. Comparatively larger intensity of this low field peak exhibited by the spectrum of glass C_4 indicates higher concentrations of isolated Cr^{3+} ions in this glass ceramic. The resonance signal at $g \sim 1.975$, arises due to the exchange coupling between Cr^{3+}–Cr^{3+} ion pairs. The intensity and the line width of this signal ($g \sim 1.97$) are found to be the highest in the spectrum of the sample C_4; such behaviour of this signal indicates the presence of larger concentration of Cr^{3+} ions in this sample. Absence of antiferromagnetic interactions between Cr^{3+} ions may also be responsible for the highest intensity of the signal to some extent in this sample [15].

As the concentration of the crystallizing agent Cr_2O_3 is increased beyond 0.4 mol%, the Cr^{3+} signals are found to

Table 2
Data on magnetic susceptibility and other related parameters of Li_2O–CaF_2–P_2O_5: Cr_2O_3 glass ceramics

Glass	χ (10^{-5}, emu)	Total chromium ion concentration N_i (10^{21}, ions/cm^3)	Cr^{3+} ion conc. evaluated from χ N' (10^{21}, ions/cm^3)	N'/N_i
C_2	5.178	2.823	2.540	0.896
C_4	10.272	5.307	5.041	0.949
C_6	12.189	8.544	5.980	0.699
C_8	12.397	11.698	6.082	0.520
C_{10}	15.525	12.696	7.617	0.599

decay (obviously due to the oxidation of Cr^{3+} ions into higher valence states) and a new weak asymmetric signal at $g = 1.983$ appeared. This signal is identified due to Cr^{5+} ions [15,17]. Earlier it was identified that it is the J–T effect that gives raise this signal of Cr^{5+} ions [18]. Thus the analysis of the results of ESR spectra predicts a possible co-existence of chromium ions in Cr^{5+} state along with Cr^{3+} state in Li_2O–CaF_2–P_2O_5: Cr_2O_3 glass ceramics especially when the concentration of the crystal stimulator is more than 0.4 mol%.

3.4. Magnetic susceptibility studies

Magnetic susceptibility of Li_2O–CaF_2–P_2O_5: Cr_2O_3 glass-ceramics measured at room temperature is observed to increase gradually with increase in the content of Cr_2O_3 (Table 2). From the values of magnetic susceptibilities, the concentration of Cr^{3+} ion is evaluated (by taking magnetic moment of Cr^{3+} ions as 3.8 μ_B) and presented in Table 2. The magnetic properties of these glasses arise from the paramagnetic Cr^{3+} ($3d^3$) ions. The fraction (N'/N_i), i.e., the ratio of Cr^{3+} ions (N') to the total concentration of the chromium ions (N_i), is found to be minimum for glass-ceramic sample C_8; this result indicates the conversion of a high proportion of chromium ions from Cr^{3+} state into Cr^{6+} state in this sample.

3.5. Dielectric properties

The dielectric constant ε' and loss $\tan\delta$ at room temperature ($\approx 30\,^{\circ}C$) of sample C_0 at 100 kHz are measured to be 8.07 and 0.0164, respectively; the values of ε' and $\tan\delta$ of all the glass-ceramic sample are found to increase slightly with decrease in frequency. Fig. 5 represents isotherms of dielectric constant (ε') with the concentration of Cr_2O_3 of Li_2O–CaF_2–P_2O_5: Cr_2O_3 glass-ceramics measured at 10 kHz. The parameter, ε' is observed to increase with the increase in the concentration of Cr_2O_3 from 0 to 0.4 mol% and for further increase (up to 0.8 mol%) the value of ε' is observed to decrease considerably at any temperature and frequency. The inset of Fig. 5 represents the variation of dielectric constant with temperature for the sample C_4 measured at different frequencies; the curves exhibit significant frequency dispersion.

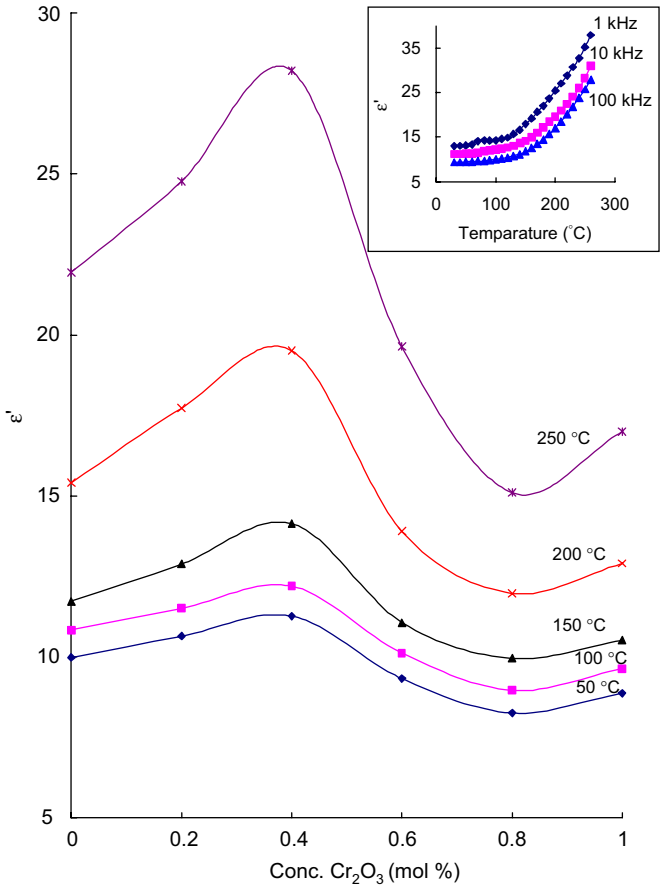

Fig. 5. Isotherms of dielectric constant variation with the concentration of Cr_2O_3 of Li_2O–CaF_2–P_2O_5: Cr_2O_3 glass-ceramics measured at 10 kHz. Inset gives the variation of dielectric constant with temperature measured at different frequencies for the sample C_4.

The dielectric constant of a material is due to electronic, ionic, dipolar and space charge polarizations. Out of these, the space charge contribution depends on the purity and the perfection of the glasses. The considerable increase of ε' with temperature of the present glasses can only be attributed to space charge polarization due to the bonding defects produced by the modifiers [19]. With the successive increase of crystallizing agent Cr_2O_3 from 0 to 0.4%, the values ε' are found to increase at any frequency and temperature indicating an increase in the space charge polarization. It is quite clear from optical absorption and ESR spectra, the chromium ions mostly exist in trivalent

state in the ceramic samples, act as modifiers similar to Li^+ and Ca^{2+} ions and generate bonding defects by breaking the P–O–P bonds. The defects thus produced create easy pathways for the migration of charges that would build up space charge polarization leading to an increase in the dielectric parameters as observed [20,21]. With the gradual increase of nucleating agent Cr_2O_3 from 0.4 to 0.8 mol%, the values of ε' are found to decrease at any frequency indicating a decrease in the space charge polarization; such a decrease may be due to the presence of a part of chromium ions in Cr^{6+} state which act as network former with CrO_4 structural units as evidenced from IR and Raman spectra. Further, there is a possibility for the cross linking of these CrO_4 units with PO_4 groups to form P–O–Cr bonds in the glass network as mentioned earlier. Such cross linkages obviously reduce the degree of disorder in the glass network and decreases the space charge polarization and leads to decrease in the values of dielectric constant of the glass ceramics.

A comparison plot of variation of dielectric loss $\tan\delta$ with temperature, measured at a frequency of 1 kHz is presented in Fig. 6. The temperature dependence of $\tan\delta$ of sample C_2 at different frequencies is shown as the inset of the same figure. The curves of all the glasses have exhibited distinct maxima; with increasing frequency the temperature maximum shifts towards higher temperature and with increasing temperature the frequency maximum shifts towards higher frequency, indicating the dielectric relaxation character of dielectric losses of these glasses. Further, the observations on dielectric loss variation with temperature for different concentrations of Cr_2O_3 clearly show a decrease in the broadness and $(\tan\delta)_{max}$ of relaxation curves with increase in the concentration of Cr_2O_3 from 0.4 to 0.8 mol%.

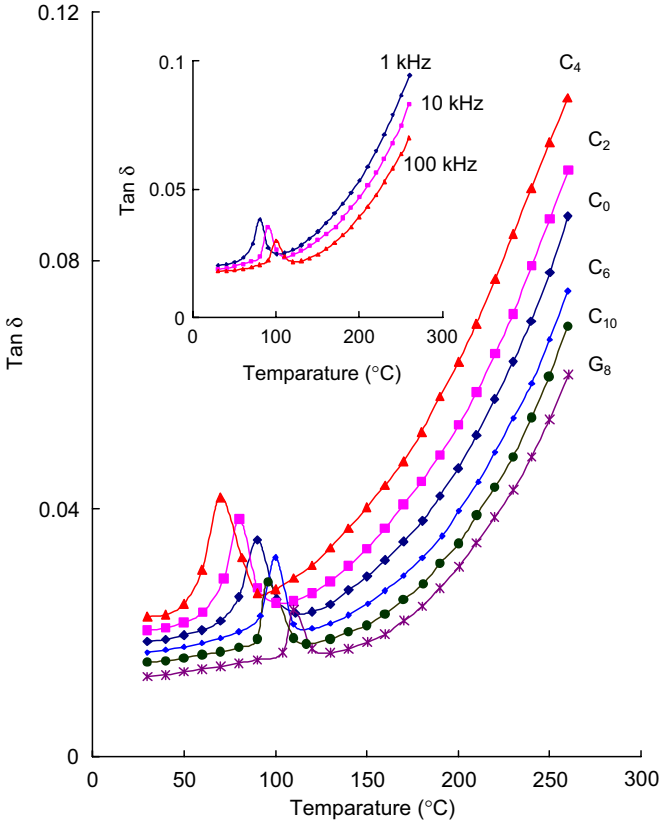

Fig. 6. A comparison plot of variation of dielectric loss with temperature for Li_2O–CaF_2–P_2O_5: Cr_2O_3 glass ceramics at 1 kHz. Inset gives the variation of dielectric loss with temperature for glass-ceramic sample C_2 at different frequencies.

Using the relation

$$f = f_O \exp(-W_d/KT), \tag{1'}$$

the effective activation energy, W_d, for the dipoles is calculated for all the glass-ceramic samples and presented in Table 3 along with the other relevant data on dielectric loss; the activation energy is found to be the highest for the sample C_8.

The observed dielectric relaxation effects in these ceramic samples may be attributed to association of divalent Ca^{2+} ions with a pair of PO_2^- in analogy with the mechanism—association of divalent positive ion with a pair of cationic vacancies—as was reported for a number of conventional glasses, glass ceramics and crystals containing divalent positive ions [22]. Although the Cole–Cole plot is very useful tool for describing relaxation effects, it is more convenient to determine the relaxation parameters by a graphical method suggested by Cole [23]. Combination of the conventional Debye's relations,

$$\varepsilon'(\omega) = \varepsilon_\infty + \frac{\varepsilon_s - \varepsilon_\infty}{1+\omega^2\tau^2}, \tag{2}$$

$$\varepsilon''(\omega) = \frac{(\varepsilon_s - \varepsilon_\infty)\omega\tau}{1+\omega^2\tau^2}, \tag{3}$$

gives rise to

$$\varepsilon''(\omega)\omega = \frac{(\varepsilon_s - \varepsilon_\infty)\omega\tau}{1+\omega^2\tau^2} = \frac{1}{\tau}(\varepsilon_s - \varepsilon'(\omega)), \tag{4}$$

$$\varepsilon''(\omega)/\omega = \frac{(\varepsilon_s - \varepsilon_\infty)\tau}{1+\omega^2\tau^2} = \tau(\varepsilon'(\omega) - \varepsilon_\infty)). \tag{5}$$

Eqs. (4) and (5) yield straight lines with slope $1/\tau$ and τ, respectively. In the present measurements for one of the ceramic samples, viz., C_4, the plots between $\varepsilon''(\omega)\omega$ vs. $\varepsilon'(\omega)$ and $\varepsilon''(\omega)\omega$ vs. $\varepsilon'(\omega)$ are shown in Fig. 7. The plots observed to be straight lines, however slight deviation from the straight line is observed in the low-frequency region.

Table 3
Data on dielectric loss of Li_2O–CaF_2–P_2O_5: Cr_2O_3 glass ceramics

Sample	$(\tan\delta)_{max\,avg}$	Temp. region of relaxation (°C)	Activation energy for dipoles (eV)
C_0	0.032	70–128	2.92
C_2	0.035	60–119	2.65
C_4	0.038	50–110	2.57
C_6	0.029	80–134	2.95
C_8	0.022	102–150	3.10
C_{10}	0.026	90–142	2.96

Such deviation suggests spreading of relaxation times. Graphs drawn for other glasses have also exhibited nearly the same behaviour. Thus the graphical analysis also indicates that in addition to the Ca^{2+} ions, there are other types of ions that are contributing to the relaxation effects. The Cr^{5+} (d^1) (probably other than those positioned in tetrahedral sites) ions also participate in dielectric relaxation effects. Earlier studies on the glasses containing d^1 ions like W^{5+}, V^{4+}, Ti^{3+}, Mo^{5+}, etc., showed that these ions act as electric dipoles and contribute to the dielectric relaxation effects [24–26]. If a part of chromium ions exists in Cr^{5+} (d^1) state (even in small concentration), they may also contribute to the relaxation effects in addition to the Ca^{2+} ions and lead to the spreading of relaxation effects. In other words, the analysis further hints out that there is a possible presence of chromium ions in Cr^{5+} state also in these samples as was indicated by the ESR spectra. The value of the effective activation energy associated with the dipoles is observed to increase with increase in the content of crystal stimulator from 0.4 to 0.8 mol% in the ceramic samples (Table 3); this observation points out a decreasing freedom for dipoles to orient in the field direction, obviously due to decreasing degree of disorder in the glass network.

The a.c. conductivity σ_{ac} is calculated at different temperatures using the equation:

$$\sigma_{ac} = \omega\varepsilon'\varepsilon_o \tan\delta, \tag{6}$$

where ε_o is the vacuum dielectric constant for different frequencies for all the glass ceramics and its variation at 10 kHz with $1/T$ is shown in Fig. 6. From these plots, the activation energy for the conduction in the high-temperature region over which a near linear dependence of $\log\sigma_{ac}$ with $1/T$ could be observed is evaluated and presented in Table 4; the activation energy is found to be the lowest for sample C_4 and highest for sample C_8. When a plot is made between $\log\sigma(\omega)$ vs. activation energy for conduction (in the high-temperature region) a near linear relationship is observed (inset (a) of Fig. 8); this observation suggests that the conductivity enhancement is directly related to the increasing mobility of the charge carriers in the high-temperature region [27]. Since the alkali earth ions, viz., Ca^{2+} ions are much less mobile than the lithium ions, the Ca^{2+} ions may therefore be regarded as virtually immobile within the time window of hopping processes of Li^+ ions [28]. Hence, the contribution to the conductivity in the present glass-ceramic samples in the high-temperature region is mainly due to the mobility of monovalent lighter lithium ions. The conductivity isotherms as a function of the concentration of nucleating agent passes through a maximum at $x = 0.4$ mol% (inset (b) of Fig. 8). The mobile electrons, or polarons, involved in the process of transfer from Cr^{3+} to Cr^{6+}, are attracted by the oppositely charged Li^+ ions. This cation–polaron pair moves together as a neutral entity. As expected, the migration of this pair is not associated with any net displacement of the charge and thus does not contribute to electrical conductivity. As a result, we expect a decrease in the conductivity, as observed in the zone II of the plots [29].

The low-temperature part of the conductivity (a near temperature independent part, as in the case of present glasses) can be explained on the basis of quantum mechanical tunneling model [30] similar to many other glass systems reported recently from our laboratory [31–33]. The value of $N(E_F)$, i.e., the density of the defect energy states near the Fermi level, is evaluated using the equation [30]

$$\sigma(\omega) = \eta e^2 KT[NE_F]^2\alpha^{-5}\omega\left[\ln\frac{\nu_{ph}}{\omega}\right]^4, \tag{7}$$

where α is the electronic wave function decay constant and its average value is determined from $\sigma_{ac} = e^{-2\alpha Ri}$, ν_{ph} is phonon frequency ($\sim 5\times 1012$ Hz), and $\eta = \pi/3$ (Austin and Mott), $\eta = 3.66\pi 2/6$ (Butcher and Hyden), $\eta = \pi 4/96$ (Pollak) and presented in Table 4.

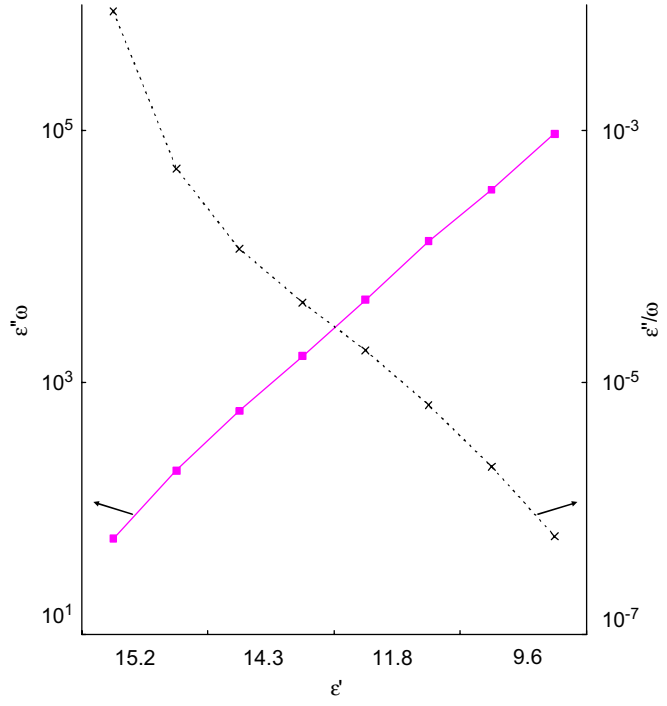

Fig. 7. Variation of the quantities $\varepsilon''\omega$ and ε''/ω with ε' of the sample C_4 at 80 °C.

Table 4
Summary of results on ac conductivity of Li_2O–CaF_2–P_2O_5: Cr_2O_3 glass ceramics

Sample	$N(E_F)$ in (10^{20}, 1/eV cm^3)			AE for conduction (eV)
	Austin–Mott	Butcher–Hyden	Pollak	
C_0	6.89	3.65	6.99	0.215
C_2	7.45	3.11	7.57	0.194
C_4	8.64	2.81	8.77	0.185
C_6	6.25	2.32	6.35	0.228
C_8	5.12	1.89	5.21	0.276
C_{10}	5.27	2.31	5.35	0.258

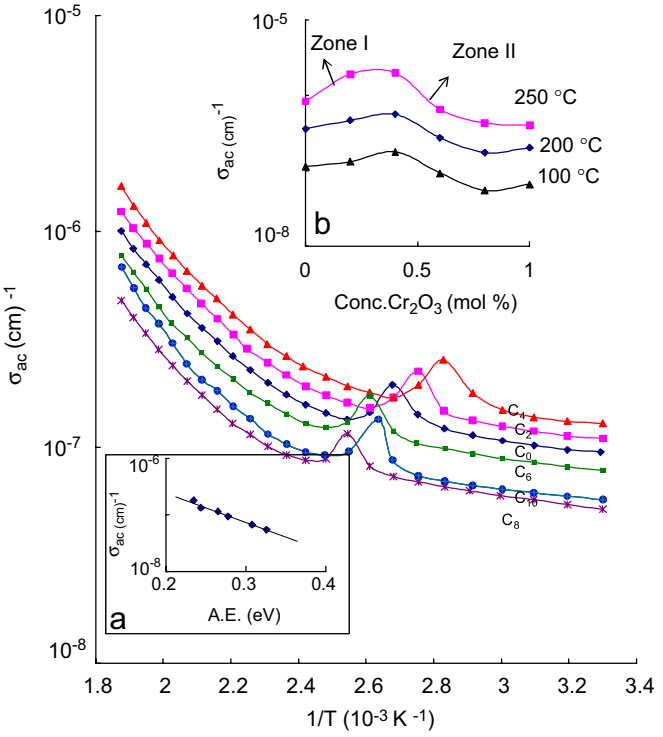

Fig. 8. A comparison plot of variation of a.c. conductivity with $1/T$ at 10 kHz for CaF_2–Li_2O–P_2O_5: Cr_2O_3 glass ceramics. Inset (a) represents the variation of conductivity with the activation energy and (b) shows the variation of conductivity isotherms with the concentration of Cr_2O_3 measured at 10 kHz.

The value of $N(E_F)$ is found to decrease with increase in the concentration of Cr_2O_3 from 0.4 to 0.8 mol% indicating a gradual increase in the rigidity of the ceramic sample.

If the applied field is an alternating field, the specific dielectric loss, i.e., the loss per unit volume of the dielectric is given by

$$\rho_1 = E^2\omega\varepsilon'\varepsilon_0 \tan\delta \,\mathrm{W/m^3}. \quad (8)$$

This equation indicates that the higher the values of $\varepsilon' \tan\delta$ of the glass at a given frequency, higher are the values of ρ_1. The dielectric breakdown strength is in fact inversely proportional to the specific dielectric loss represented by Eq. (8). Our observations on dielectric parameters of Li_2O–CaF_2–P_2O_5: Cr_2O_3 glass ceramics, as mentioned earlier, indicate, the rate of increase of $\varepsilon' \tan\delta$ with temperature is the lowest for the sample C_8; the breakdown strength, which is inversely proportional to $\varepsilon' \tan\delta$ is therefore expected to be the highest when compared with the other glass ceramics. Thus the experiments on the dielectric breakdown strength of Li_2O–CaF_2–P_2O_5: Cr_2O_3 glass ceramics reveal that the sample C_8 possesses high electrical insulating strength among all other samples studied.

4. Conclusions

The summary of the data from the study of various physical properties of Li_2O–CaF_2–P_2O_5: Cr_2O_3 glass ceramics is as follows: The optical absorption and ESR spectral studies indicate that there is a gradual conversion of chromium ions from Cr^{3+} state to Cr^{6+} state as the concentration of the nucleating agent is increased from 0.4 to 0.8 mol%. The presence of chromium ions in Cr^{4+} and Cr^{5+} states could also be felt from these studies. The glass-ceramic samples crystallized with 0.4 mol% Cr_2O_3 (in which chromium ions exists predominantly in Cr^{3+} state) exhibited high luminescence emission and hence these samples may be considered as more efficient luminescence materials. Though a part of the chromium ions seems to exist in Cr^{4+} state in the sample C_8, that give laser emission in the NIR range, but their concentration is very low and further there is a possibility of high non-radiating or phonon losses in this sample. The dielectric studies indicate the highest insulating strength for the sample C_8 and the a.c. conduction in the samples C_2 and C_4 is primarily ionic in nature.

References

[1] L. Bih, M. El Omari, J.-M. Reau, M. Haddad, D. Boudlich, A. Yacoubi, A. Nadiri, Solid State Ion. 132 (2000) 71.
[2] V.A. Trepakov, M.E. Savinov, O. Okhay, A. Tkach, P.M. Vilarinho, A.L. Kholkin, I. Gregora, L. Jasstrabik, J. Eur. Ceram. Soc. (2007), doi:10.1016/j.jeurceramsoc.2007.02.022.
[3] K. Yukimitu, E.B. Araújo, J.C.S. Moraes, V.C.S. Reynoso, C.L. Carvalho, J. Phys. D-Appl. Phys. 35 (2002) 3229.
[4] R.A. Montani, M.A. Frechero, Solid State Ion. 158 (2003) 327.
[5] G. Murali Krishna, N. Veeraiah, N. Venkatramaiah, R. Venkatesan, J. Alloys Compd. Part-I (2006).
[6] Weifeng Li, Xiqi Feng, Yidong Huang, Zundu Luo, Wenliang Zh, J. Lumin. 113 (2005) 109.
[7] A.M. Malyarevich, Yu.V. Volk, K.V. Yumashev, V.K. Pavolvskii, S.S. Zapalova, O.S. Dymshits, A.A. Zhilin, J. Non-Cryst. Solids 351 (2005) 3551.
[8] S. Ram, K. Ram, B.S. Shukla, J. Mater. Sci. 27 (1992) 511.
[9] H. Yuan, D. Cohen, B.G. Aitken, Mater. Res. Soc. Symp. Proc. 455 (1997) 483.
[10] Cz. Koepke, K. Winsneiwski, M. Grinberg, T.P.J. Han, A. Majchrowski, J. Phys.: Condens. Matter 13 (2001) 2701.
[11] A.B. Bykov, M.Yu. Sharonov, V. Petricevic, I. Popov, L.L. Isaacs, J. Steiner, R.R. Alfano, J. Non-Cryst. Solids 352 (2006) 5508.
[12] L.P. Sosman, T. Abritta, O. Nakamura, M.F. D'Aguiar Neto, J. Mater. Sci. Lett. 14 (1995) 19.
[13] V. Ramesh Kumar, J.L. Rao, N.O. Gopal, J. Mater. Sci. 41 (2006) 2045.
[14] A. Majchrowski, I.V. Kityk, J. Ebothé, Phys. Status Solidi (b) 241 (2004) 3047.
[15] I. Ardelean, S. Filip, J. Optoelectron. Adv. Mater. 7 (2005) 745.
[16] I. Ardelean, O. Cozar, V. Simon, S. Filip, J. Magn. Magn. Mater. 157 (1996) 165.
[17] T.S.N. Murthy, V. Srinivas, G. Saibabu, M. Salagram, J. Solid State Chem. 97 (1992) 358.
[18] M. Srinivasa Reddy, S.V.G.V.A. Prasad, N. Veeraiah, Phys. Status Solidi (a) 204 (2007) 816.
[19] G. Srinivasarao, N. Veeraiah, J. Solid State Chem. 166 (2002) 104.
[20] N. Krishna Mohan, G. Sahaya Baskaran, N. Veeraiah, Phys. Status Solidi (a) 203 (2006) 2083.
[21] P. Subbalakshmi, P.S. Sastry, N. Veeraiah, Phys. Chem. Glasses 42 (2001) 307.
[22] P. Subbalakshmi, N. Veeraiah, J. Non-Cryst. Solids 298 (2002) 89.
[23] C.J.F. Bottcher, P. Bordewijk, Theory of Electric Polarization, vol. 2, Elsevier Scientific Publishing Company, Amsterdam, 1978.
[24] R.M. Abdelouhab, R. Braunstein, K. Baerner, J. Non-Cryst. Solids 108 (1989) 109.

[25] R. Balaji Rao, D. Krishna Rao, N. Veeraiah, Mater. Chem. Phys. 87 (2004) 357.
[26] G. Srinivasarao, N. Veeraiah, Phys. Status Solidi (a) 191 (2002) 370.
[27] G. El-Damrawi, J. Phys.: Condens. Matter 7 (1995) 1557.
[28] S.R. Elliott, Adv. Phys. 36 (1987) 135.
[29] J.C. Bazan, J.A. Duffy, M.D. Ingram, M.R. Mallace, Solid State Ion. 86–88 (1996) 497.
[30] I.G. Austin, N.F. Mott, Adv. Phys. 18 (1969) 657.
[31] G. Murali Krishna, N. Veeraiah, N. Venkatramaiah, R. Venkatesan, J. Alloys Compd. Part II (2006), doi:10.1016/j.jallcom.2006.10.148.
[32] N. Krishna Mohan, C.K. Jayasankar, N. Veeraiah, J. Alloys Compd. (2007), doi:10.1016/j.jallcom.2007.04.143.
[33] M. Srinivasa Reddy, V.L.N. Sridhar Raja, N. Veeraiah, Eur. Phys. J. Appl. Phys. (2007), doi:10.1051/epjap:2007022.